Advances in $CuInSe_2$-based Solar Cells: From Fundamentals to Processing

W. Shafarman, J. Titus, M. Haimbodi, M. Gossla, G. Hanket, S. Marsillac, T. Minemoto,
P. Paulson, B. Sang, U. Singh, E. Eser, R. Birkmire
Institute of Energy Conversion, University of Delaware, Newark, DE 19716

ABSTRACT

Recent progress is reported on a range of issues critical to the fundamental understanding of materials, devices, and processing of $CuInSe_2$-based thin films. Materials related results include characterization of the optical properties of $Cu(InGa)Se_2$ using spectroscopic ellipsometry, the diffusion of S into $Cu(InGa)Se_2$, and the growth and characterization of $CuAlSe_2$ films. Results on wide bandgap devices include alloys of $CuInSe_2$ with Al, Ga, and S along with different bandgap buffer layers. Finally, progress on the roll-to-roll deposition of $Cu(InGa)Se_2$ on a flexible web is reported.

1. Introduction

While there has been impressive progress in the performance of $Cu(InGa)Se_2$ solar cells and modules there remains a significant need to develop a greater fundamental science and engineering basis for $Cu(InGa)Se_2$ materials, devices, and processing requirements. There is a particular need for more fundamental understanding of wide bandgap alloys and devices since these should lead to improved module performance and could enable the development of thin film based tandem cells. The latter would likely require cells with absorber alloys having $1.5 \leq E_g \leq 1.9$ eV for the top cells.

In this paper, recent progress on a range of critical issues is reported. This includes a fundamental study of the optical properties of $Cu(InGa)Se_2$ using spectroscopic ellipsometry. The diffusion of S into $Cu(InGa)Se_2$ which has been used to modify the bandgap, and the growth and characterization of $CuAlSe_2$ films to provide the basis for work on $Cu(InAl)Se_2$ alloys are addressed. Advances in the understanding of processing, materials, and devices based on $Cu(InGa)(SeS)_2$ and $Cu(InAl)Se_2$ wide bandgap alloys are reported. Growth of (CdZn)S and ZnS buffers has been developed as a tool to study junction formation with wide bandgap $CuInSe_2$ based alloy absorber layers. Finally, the deposition of $Cu(InGa)Se_2$ in a continuous, roll-to-roll process is potentially an advantageous process for large scale manufacturing and processing improvements and device results are reported.

2. Optical characterization

Variable angle spectroscopic ellipsometry (SE) has been used to complete a detailed characterization of the fundamental optical constants of $Cu(InGa)Se_2$ polycrystalline thin films as a function of the relative Ga content $x \equiv Ga/(In+Ga)$ over an energy range from 0.75 to 4.6 eV. This provides a basis for evaluating the $Cu(InGa)Se_2$ band structure and input for device models using optical constants measured directly on films similar to those used in high efficiency solar cells. In addition, this data provides the basis for potential utilization of SE as an in-situ or in-line diagnostic tool.

A series of single phase $Cu(InGa)Se_2$ films with uniform composition through the film thickness was deposited by elemental evaporation. Due to their high surface roughness, as-deposited films are generally not suitable for ellipsometer measurements. So, the measurements were carried out on the reverse side of the films immediately after peeling them from the Mo-coated soda lime glass substrates. Prior to peeling the film, an optically thick Mo film was deposited on the exposed $Cu(InGa)Se_2$ surface so that the back surface during measurements was well defined. XPS measurements confirmed that the peeled $Cu(InGa)Se_2$ surface contained no Mo or $MoSe_2$. A detailed multilayer optical model of the ellipsometric data, generic to ternary chalcopyrite films, was developed to determine the refractive index and extinction coefficient. The optical model consists of: 1) surface roughness on the peeled layer; 2) the $Cu(InGa)Se_2$ film; 3) an interface layer (surface layer before peeling); and 4) the Mo layer. The surface roughness determined by the analysis is comparable to that measured by atomic force microscopy.

The resulting optical constants measured on polycrystalline $CuIn_{1-x}Ga_xSe_2$ films were found to be comparable to the ordinary component (electric field perpendicular to the crystal c-axis) of the single crystal optical constants indicating that the polycrystalline nature of the film did not affect the optical constants. Particular effort was made to obtain high resolution data in the region very close to the bandgap. This enabled determination of the fundamental transitions $E_0(A)$, $E_0(B)$, and $E_0(C)$ which result from crystal field and spin orbit splittings of the valence band maximum. The evolution of these energies with x is shown in Figure 1. The bandgap corresponding to the lowest energy transition $E_0(A)$ can be fit by $E_g = 1.038 + 0.38x + 0.27x^2$, i.e. with a bowing parameter = 0.27.

3. Wide bandgap materials: S-diffusion

The partial replacement of Se with S in the surface region of $Cu(InGa)Se_2$ films can reduce the diode current in solar cells while leaving the light-generated current unchanged. Optimization of this effect requires an understanding of the S incorporation process into the absorber layer.

Sulfur reaction is typically performed by annealing the sample at atmospheric pressure for 1 hour at 575°C in 2% H_2S with balance Ar. At the present time, only samples without Ga have been used. In an effort to eliminate grain boundary and substrate effects, polished single-crystal samples grown by various methods were sulfurized. These crystals were grown by either a vertical gradient freeze

(VGF) or by a traveling heater (TH) method. During TH growth either In or CuSe were used as solvents. The reacted samples were analyzed with the use of SEM, EDS and XRD.

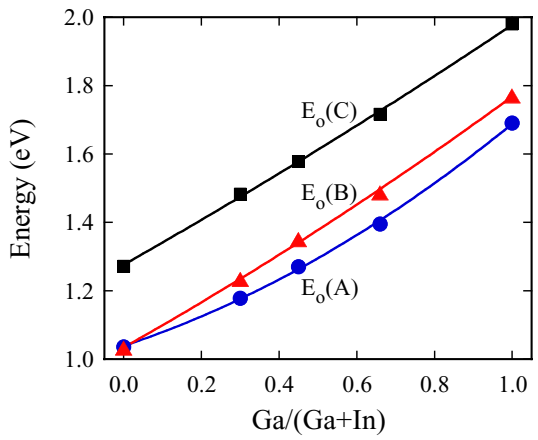

Figure 1. Effect of increasing Ga content on the fundamental optical transitions in $Cu(InGa)Se_2$ thin films.

VGF and TH(CuSe) grown crystals remained relatively smooth after the sulfur reaction process, in contrast to TH(In) grown crystals. Additionally, the TH(In) crystals incorporated substantially more S than the other crystal types. EDS on TH(In) crystals after sulfurization resulted in S/(Se+S) values of 0.73 compared to values of about 0.04 for the other crystal types. Cross-sectional SEM on such a crystal showed a rough surface layer on top of an undisturbed crystalline bulk. XRD in Bragg-Brentano geometry featured clearly distinguished $CuIn(SeS)_2$ peaks, indicating that this surface layer is polycrystalline.

Efforts are underway to understand these differences in reaction with H_2S which may result from differences in the initial Se content of the various crystals. Subsequently, the results will be used to determine the bulk diffusion constant for S in $CuInSe_2$, leading to a quantitative understanding of the sulfurization process for both crystal and film samples.

4. Wide bandgap materials: $CuAlSe_2$

Great progress has been achieved with $Cu(InAl)Se_2$ based solar cells, resulting in efficiencies as high as 16.9% [1], and will be discussed in the next section. However, with Al/(In+Al) > 0.6 significant amounts of oxygen are incorporated in the $CuInAlSe_2$ films [2]. To understand the origin of the O in the films and provide a foundation for the $Cu(InAl)Se_2$ alloy materials, growth of $CuAlSe_2$ films has been investigated.

$CuAlSe_2$ films were deposited by multisource elemental evaporation in which the Cu, Al and Se incident fluxes were varied so that the Cu/Al ratio ranged from 0.3 to 1.5 and the Se/(Cu +Al) ranged from 2 to 20. Films grown with the Cu/Al incident flux ratio from 0.3 — 1.2 and Se/(Cu+Al) from 2 — 4, comparable to that typically used during $Cu(InGa)Se_2$ deposition, contained Cu-Al intermetallic compounds and high concentration of O. The observed Cu-Al compounds, Cu_2Al, CuAl and $CuAl_2$, systematically varied with decreasing Cu/Al incident flux ratio. Similarly, O in the films increased with decreasing Cu/Al flux. It is assumed that Al_xSe_y, which is thermodynamically favored, forms during film growth and reacts with atmospheric oxygen and water vapor upon removal from the deposition system. These results suggest a steady state growth of Cu-Al alloys and Al_xSe_y under these conditions. There is no Cu-Al-Se phase diagram available to indicate whether this is an equilibrium condition or is kinetically controlled

Films deposited with very large Se flux, such that Se/(Cu+Al) > 10, and Cu/Al from 0.6 — 1.2 had optical bandgap E_g = 2.7 eV, equal to that of $CuAlSe_2$. However, XRD measurements show a shift in the (112) reflection from that for chalcopyrite $CuAlSe_2$ and additional, unidentified reflections. Glancing angle XRD measurements revealed identical intensity patterns at different sampling depths, indicating that the films uniformly contain a new $CuAlSe_2$ phase. Annealing films with this new phase in H_2Se, Ar or H_2/Ar at temperatures from 450—550° C transforms them to chalcopyrite $CuAlSe_2$. However, the O concentration increases with annealing suggesting that the anneal results in a mixed $CuAlSe_2$-Al_xSe_y film and the Al_xSe_y compound reacts in air. Finally, films grown with Cu/Al > 1.2 contained $CuAlSe_2$ and $CuSe_2$ phases with the O concentration less than 2 %, independent of the relative Se flux.

These results indicate that the formation of $CuAlSe_2$ is kinetically controlled by the delivery of Cu, Al, and Se species to the substrate surface. It cannot be determined if the Cu-Al alloys exist in equilibrium with Al_2Se without a detailed phase diagram. However, these results provide an approach to growing $Cu(InAl)Se_2$ films with Al/(In+Al) > 0.6 by using a high Se flux.

5. Wide bandgap devices: $Cu(InAl)Se_2$

High efficiency $Cu(InAl)Se_2$ based solar cells have been achieved using absorber layers deposited by multisource elemental evaporation with a uniform deposition process at T_{SS} = 530°C. The best cell efficiency, 16.9%, was obtained with a film that had Al/(In+Al) = 0.13 and E_g = 1.16 eV [1]. The morphology and structure observed by SEM and XRD characterization showed no differences other than a lattice parameter shift between $Cu(InAl)Se_2$ and $Cu(InGa)Se_2$. J-V and QE behavior was nearly identical to that of a $Cu(InGa)Se_2$ cell with Ga/(In+Ga) = 0.26.

A critical improvement in the cell process that enabled this high efficiency was improved adhesion between the Mo back contact and the $Cu(InAl)Se_2$ resulting from a thin, 5 nm, Ga layer sputter-deposited on the Mo prior to $Cu(InAl)Se_2$ deposition [1]. Without this Ga layer, the adhesion of $Cu(InAl)Se_2$ films deposited with T_{SS} > 450° C was insufficient for cell fabrication. Even with the Ga interlayer, occurrences of delamination at the Mo/$Cu(InAl)Se_2$ interface during cell fabrication increased for relative Al content of Al/(In+Al) > 0.3 or E_g > 1.4 eV. Therefore, variations in the $Cu(InAl)Se_2$ deposition process which could further improve adhesion have been investigated. A thin, ~5 nm, Cu layer evaporated onto the

Mo at the start of the $Cu(InAl)Se_2$ process provided similar benefits to the sputtered Ga layer. However, a bi-layer evaporation process which began with Cu-rich $Cu(InAl)Se_2$ did not further improve adhesion when the Ga interlayer was incorporated and gave comparable film and device characteristics to the uniform process. Evaporation processes which began with an In-Al-Se layer always had very poor adhesion and no devices were fabricated.

The $Cu(InAl)Se_2$ bandgap was varied from 1.1 to 1.7 eV by increasing Al/(In+Al) from 0 to 0.5 [3]. The efficiency of the resulting devices decreased for $E_g > 1.2$ eV. Characterization of the solar cells showed that their limiting behavior was similar to that in $Cu(InGa)Se_2$. Temperature dependent J-V measurements showed that $V_{OC} \rightarrow E_g$ as $T \rightarrow 0$ and analysis of the J-V data showed diode quality factors $1.5 < A < 2$. This behavior is characteristic of a device limited by Shockley-Read-Hall recombination in the absorber layer. As E_g increased beyond 1.2 eV, the device efficiency decreased and V_{OC} did not increase beyond 0.76 V. Differences between the light and dark J-V measurements and voltage dependent QE measurements showed that the higher bandgap devices were also limited by poor collection of light generated carriers.

6. Wide bandgap devices: $Cu(InGa)(SeS)_2$

Evaporated $Cu(InGa)(SeS)_2$ films are also being developed for wide bandgap solar cells. In this case, E_g can be continuously varied by changing either the relative Ga/In or S/Se compositions. Solar cells based on either $Cu(InGa)Se_2$ or $CuIn(SeS)_2$ with E_g greater than about 1.3 eV have decreasing performance as E_g increases further. In the pentenary material $Cu(InGa)(SeS)_2$, the cation and anion alloying concentrations can be kept to a minimum.

Evaporation of $Cu(InGa)(SeS)_2$ required a deposition system to be constructed with 2 special concerns different than a typical system used for $Cu(InGa)Se_2$ evaporation. First, the chalcogen sources were designed to provide independent control at temperatures in the range 100 — 350°C even when the other metal sources are operating at 1000 — 1400°C. Second, the system was constructed to withstand the corrosive effects of S vapor.

$Cu(InGa)(SeS)_2$ films have been deposited with a wide range of deposition conditions, including T_{SS} and relative fluxes. Figure 2 shows the ratio S/(Se+S) in the film, measured by EDS, as a function of S/(Se+S) in the vapor during the deposition for samples deposited at T_{SS} = 400 and 550°C. In all cases the Cu, Ga, and In fluxes were constant through the deposition and all films were Cu-poor with Cu/(In+Ga) ≈ 0.8 — 1.0. The data alllies on one curve, independent of substrate temperature and Ga/(In+Ga) ratio which varied from 0.2 — 0.5. The films preferentially incorporate Se resulting in the need to precisely deliver very high S/Se flux to incorporate higher amounts of sulfur in the films. A curve in Figure 2 shows a fit suggested by an equilibrium thermodynamic model [4].

An approach to forming $Cu(InGa)(SeS)_2$ films with uniform composition through their thickness, but without precise S/Se flux control, was to sequentially deposit layers with only S or Se using conditions in which the layers intermix. Sequential depositions were done with In-Ga-Se or In-Ga-S followed by Cu-S or Cu-Se so that the final composition had Cu > (In+Ga). The resulting Cu_xS_y, or Cu_xSe_y phase, was selectively etched from the final film. It was believed that these Cu-rich phases might act to enhance intermixing during growth, but Auger depth profile measurements indicate that the chalcogen species remained segregated and XRD measurements showed two distinct chalcopyrite phases. Devices were fabricated and J-V and QE measurements behaved like either $Cu(InGa)Se_2$ or $Cu(InGa)S_2$, depending on the deposition sequence

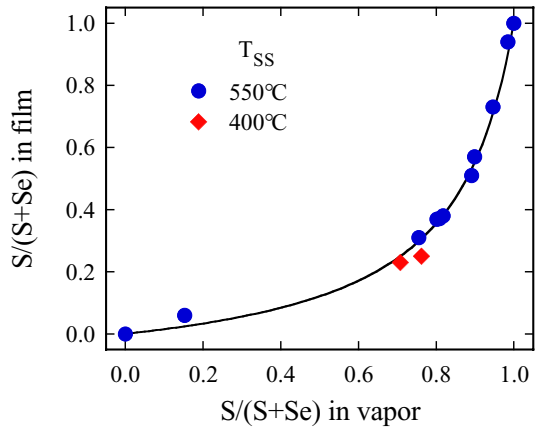

Figure 2. Relative S incorporation in evaporated $Cu(InGa)(SeS)_2$ films.

Devices were also fabricated using a set of $Cu(InGa)(SeS)_2$ films with $0 \le S/(Se+S) \le 1$ and the relative Ga/(In+Ga) concentration varied to maintain a bandgap of 1.55 – 0.05 eV. This is roughly the minimum bandgap that might be used in a tandem structure and enables one endpoint in the set of films to be the ternary $CuInS_2$ compound. All films were deposited with indium rich composition in a single step deposition at substrate temperature 550°C. Therefore, no KCN etching was done on the films as has been used in processing the highest efficiency $CuInS_2$ devices. The highest cell efficiency, η = 9.4%, was obtained with no S and Ga/(In+Ga) = 0.73. However, V_{OC} increased from 808 to 854 mV when S/(Se+S) increased to 0.26, but efficiency decreased to 7.4%. With higher S concentration the device efficiency dropped off sharply.

7. Junction characterization: ZnS and (CdZn)S

Chemical bath deposition of ZnS and (CdZn)S has been developed to enable the band alignment and chemistry at the $Cu(InGa)Se_2$ / buffer layer interface to be controlled. Characterization of devices with different buffer layers will be used to determine the effects of the interface on device performance.

ZnS was deposited from solutions of $ZnSO_4$, thiourea and ammonia [5]. Differences in equilibrium reaction constants with Zn compared to Cd necessitated different reaction conditions from those used for CdS deposition. The effects of independently varying the concentrations of

each constituent were characterized and conditions determined to optimize the growth rate and form a dense adherent film. Too great a concentration of $ZnSO_4$ or too small an ammonia concentration resulted in colloidal growth with precipitates forming in the bath and on the film surface so the film was porous or discontinuous. Under optimum conditions, ZnS films with thickness 50 nm could be obtained in < 40 min at an 80°C bath temperature. XRD and optical measurements showed that the films were microcrystalline with cubic structure and E_g = 3.6 eV. The best $Cu(InGa)Se_2$ solar cell using the ZnS buffer had 13.9% efficiency and the J-V parameters are compared to the control device with a CdS buffer layer in Table 1. The ZnS buffer layer resulted in an increased J_{SC} with higher quantum efficiency at short wavelengths but V_{OC} and FF were lower than those with the CdS buffer. To obtain this device performance using the ZnS required annealing the $Cu(InGa)Se_2$/ZnS structure in air at 150°C for 30 min prior to the deposition of TCO and grid layers.

(CdZn)S films have also been deposited by chemical bath deposition in which the $CdSO_4$ is partially replaced by $ZnSO_4$. Formation of the single phase alloy required the bath temperature, pH and deposition time to be adjusted. Films were deposited with bandgap up to 2.66 eV, as determined by spectroscopic ellipsometry. The compositions are difficult to determine by EDS because the films are < 100 nm thick. $Cu(InGa)Se_2$ cell results, also shown in Table 1, indicate that comparable cell performance was obtained with CdS or (CdZn)S.

Table 1. $Cu(InGa)Se_2$ cell results with CdS and (CdZn)S buffer layers.

Buffer layer	E_g (eV)	η (%)	V_{OC} (mV)	J_{SC} (mA/cm^2)	FF (%)
CdS	2.4	15.0	660	31.3	72.4
ZnS	3.6	13.9	618	32.4	69.3
CdS	2.4	13.6	615	30.6	72.2
(CdZn)S	2.66	13.6	603	31.1	72.6

8. Roll-to-Roll $Cu(InGa)Se_2$ deposition

The interest in lightweight flexible PV modules from various end-users coupled with potential cost advantages of continuous roll-to-roll manufacturing of thin-film modules led to the initiation of a development program for the deposition of $Cu(InGa)Se_2$ films on Mo coated high temperature Upilex S polyimide (PI) films [6]. However, a number of factors which might limit the performance had to be accepted from the start: 1) the maximum substrate temperature is limited to ~ 450°C; 2) no Na is available from the substrate for incorporation into the $Cu(InGa)Se_2$ film; and 3) the sequential evaporation may result in undesirable composition gradients in the film.

The in-line system, described in [6], consists of a roll-to-roll web drive, backside substrate heating of the substrate, and sequentially placed Cu, Ga, and In evaporation sources. Se is delivered globally via a sparger. The Cu and In sources are controlled by atomic absorption spectroscopy, while Ga and Se are controlled by temperature. The substrate web moves through the deposition zone in 20 min for film thicknesses in the range of 2 to 3 μm. At the present time Mo-coated 6" wide PI substrate is provided by Global Solar Energy.

Poor adhesion of the $Cu(InGa)Se_2$ film to the Mo was one of the early challenges faced in the program. A solution to this problem was found in the deposition of a thin precursor layer of $Ga_{2-x}In_xSe_3$, where x is small enough that XRD shows a pattern consistent with β-Ga_2Se_3 in which the peaks are shifted to higher d-values due to substitutional In. Improved adhesion with this precursor layer allowed the characterization of the process uniformity and reproducibility in terms of device efficiency metrics. Eleven small area samples, with 4 devices each, made from $Cu(InGa)Se_2$ deposited over 5ft of PI/Mo showed an average efficiency of 9.2% with a standard deviation of 1.0%. The best device efficiency for 12 different runs averaged around 10% even though the Cu/(In+Ga) ratio varied from 0.7 to 0.9 indicating a large operational window despite the absence of Na in the films.

During the roll-to-roll deposition of $Cu(InGa)Se_2$ onto PI/Mo, web cracking of the Mo layer has been observed to various degrees. This in turn resulted in the duplication of the same cracking pattern in the $Cu(InGa)Se_2$ layer. In one PI/Mo web substrate no cracking was observed while in others the cracking was heavy enough that operational devices could not be fabricated. The problem, being investigated further, is related to the Mo deposition process which has not been optimized for the $Cu(InGa)Se_2$ deposition environment where the web is under tension at a temperature of ~ 450°C.

Acknowledgment

This work was supported by the National Renewable Energy Laboratory under the Thin Film Partnership Program (subcontract ADJ-1-30630-12) and under the High Performance PV Program (subcontract AAT-1-30620-07).

References

[1] S. Marsillac, P.D. Paulson, M.W. Haimbodi, R.W. Birkmire and W.N. Shafarman, *Appl. Phys. Lett.* **81**, 1350 (2002).

[2] M. W. Haimbodi, E. Gourmelon, P. D. Paulson, R. W. Birkmire, and W. N. Shafarman, Proc. 28th IEEE PVSC, 454 (2000).

[3] W. N. Shafarman, S. Marsillac, P. D. Paulson, M. W. Haimbodi, T. Minemoto, and R. W. Birkmire, Proc. 29th IEEE PVSC, 519 (2002).

[4] R. Birkmire and M. Engelmann, AIP Conf. Proc. 462, 23 (1998).

[5] B. Sang, W. N. Shafarman, and R. W. Birkmire, Proc. 29th IEEE PVSC, 632 (2002).

[6] G. M. Hanket, U. P. Singh, E. Eser, W. N. Shafarman, and R. W. Birkmire, Proc. 29th IEEE PVSC, 567 (2002).